

Seismic swarm intelligence inversion with sparse probability distribution of reflectivity



Zhiguo Wang^{a,*}, Bing Zhang^b, Zhaoqi Gao^b, Jinghuai Gao^b

^a School of Mathematics and Statistics, Xi'an Jiaotong University, Xi'an, Shaanxi, 710049, PR China

^b School of Information and Communications Engineering, Xi'an Jiaotong University, Xi'an, Shaanxi, 710049, PR China

ARTICLE INFO

Keywords:

Seismic inversion
Swarm intelligence
Differential evolution
Particle swarm optimization
Sparse distribution

ABSTRACT

Seismic inversion, such as velocity and impedance, is an ill-posed problem. To solve this problem, swarm intelligence (SI) algorithms have been increasingly applied as the global optimization approach, such as differential evolution (DE) and particle swarm optimization (PSO). Based on the well logs, the sparse probability distribution (PD) of the reflectivity distribution is spatial stationarity. Therefore, we proposed a general SI scheme with constrained by a priori sparse distribution of the reflectivity, which helps to provide more accurate potential solutions for the seismic inversion. In the proposed scheme, as two key operations, the creating of probability density function library and probability transformation are inserted into standard SI algorithms. In particular, two targeted DE-PD and PSO-PD algorithms are implemented. Numerical example of Marmousi2 model and field example of gas hydrates show that the DE-PD and PSO-PD estimate better inversion solutions than the results of the original DE and PSO. In particular, the DE-PD is the best performer both in terms of mean error and fitness value of velocity and impedance inversion. Overall, the proposed SI with sparse distribution scheme is feasible and effective for seismic inversion.

1. Introduction

Seismic inversion is an important area of geophysical research in regional, global and exploration problems. Using artificial or natural seismic data, the seismic inversion estimates unknown subsurface parameters, such as velocity, density, quality factor, impedance, and reflectivity. Due to the band-limited nature of the source wavelet, the acquired seismic data is typically band-limited. Consequently, the seismic inversion is ill-posed (Wang, 2011; Wang et al., 2018). To solve this problem, additional assumptions on the model parameters are required. For example, the sparsity assumption is popular to solve the seismic inversion (Gholami and Sacchi, 2015; Kazemi et al., 2016; Zhou et al., 2015), especially for the earth model of layered medium.

To solve the seismic inverse problem, the classical optimization algorithms based on gradient descent is sensitive to the initial model and easy to be trapped in a local minimum (Ma, 2002). In addition, it is difficult and time-consuming to fine tune the regularization parameters to obtain a fast convergence rate (Zhou et al., 2015; Pan et al., 2020).

In contrast to the gradient-based optimization algorithms, the global optimization approaches do not require the computation of the gradient or an accurate initial model. Global optimization has been increasingly

applied to geophysical problems (Sen and Stoffa, 2013). Swarm intelligence (SI) algorithms are a set of global optimization approaches. SI is the collective behavior of decentralized, self-organized systems that often are inspired by biological systems such as ant colonies, bird flocking, and fish schooling (Blum and Merkle, 2008). Many SI algorithms have been introduced and successfully applied over the past decades. For example, differential evolution (DE) and particle swarm optimization (PSO) are two notable SI algorithms. DE is a popular robust and efficient SI algorithm (Storn and Price, 1997). On the other hand, PSO is another optimization algorithm due to its simplicity and efficiency (Kennedy and Eberhart, 1995). In geophysical inversion, DE and PSO algorithms have been widely used since the early 1990s (Semanian et al., 2009; Wang and Gao, 2012; Gao et al., 2014; Gao et al., 2016; Wardhana and Pranowo, 2022).

To obtain the unknown subsurface parameters, the SI algorithm searches directly for a solution in a search space \mathbb{S} of candidate solutions. In the case of constrained optimization, a solution is found in the feasible region \mathbb{f} , where $\mathbb{f} \subseteq \mathbb{S}$. If the probability distribution (PD) of the solution is known, the \mathbb{f} is easy to construct. But the analytical PD of the parameters is undefined for the seismic data. On the other hand, well logs including acoustic and density can be obtained from the subsurface

* Corresponding author.

E-mail address: emailwzg@gmail.com (Z. Wang).

resource exploration and the earth deep drilling in the continent and ocean. Considering the layered earth model, the sparsity assumption of reflectivity is feasible. In a depositional area, a probability density function (PDF) of the reflectivity can be estimated from the acoustic and density logs of a well. In the same depositional area, the reflectivity distribution can be assumed to be spatial stationarity. Therefore, based on the PDF of reflectivity, the shape of the \mathbf{f} can be constrained, providing more accurate potential solutions for the seismic inversion.

In this study, we proposed the scheme of the SI algorithms with PD constraint, such as sparse distribution, to solve the seismic inversion problem. For the sake of comparison, we focus on two SI algorithms including DE and PSO with PD constraint, named DE-PD and PSO-PD respectively. In this scheme, we construct a probability transformation that keeps the distribution of the model parameter as the same as the PD of the well data due to the spatial stationarity of the reflectivity distribution. Under the same condition, numerical and field examples show that the DE-PD and PSO-PD estimate better inversion solutions than the results of the conventional DE and PSO. In particular, the DE-PD is the best performer in the seismic inversion.

2. Method

2.1. Seismic inversion problem

In 1D seismic inversion, unknown subsurface parameters \mathbf{m}_{true} are typically estimated by minimizing a waveform misfit function J between model data \mathbf{d} and observation data \mathbf{d}_{obs} . The form of $J : \mathbb{R}^N \rightarrow \mathbb{R}$ can be expressed as

$$J = \|\mathbf{d} - \mathbf{d}_{obs}\|_q^q, \quad (1)$$

$$\mathbf{d} = \mathcal{T}(\mathbf{m}), \quad (2)$$

$$\mathbf{d}_{obs} = \mathcal{T}(\mathbf{m}_{true}) + \mathbf{n}, \quad (3)$$

where $q > 0$, \mathbf{n} denotes the additive noise, and \mathcal{T} denotes a mapping operator between the model \mathbf{m} and the data \mathbf{d} . For the layered earth model, \mathbf{m} denotes the earth's reflectivity. The reflectivity of i th layer can be calculated by

$$m_i = \frac{I_{i+1} - I_i}{I_{i+1} + I_i}, \quad (4)$$

where I_i denotes the seismic impedance. The seismic impedance can be written as

$$I_i = \rho_i v_i, \quad (5)$$

where ρ_i denotes the density of a rock, and v_i denotes the compressional wave velocity.

Sometimes, the density can be simplified as a constant in a seismic inversion. Therefore, the velocity, impedance and reflectivity can be estimated by using seismic inversion in the layered earth model, respectively. The choice of inversion parameters of the earth model mainly depends on the detailed geological challenge.

To solve this inversion problem, the estimation of \mathbf{m} usually can be reformulated by an optimization problem

$$\min_{\mathbf{m} \in \mathbb{R}^n} \|\mathbf{m}\|_p^p, \text{ s.t. } \|\mathbf{d} - \mathbf{d}_{obs}\|_2^2 \leq \sigma^2, \quad (6)$$

where $p > 0$, $\|\mathbf{m}\|_p^p := \sum_{i=1}^n |m_i|^p$, denotes the ℓ_p norm (if $p \geq 1$) or quasi norm (if $0 < p < 1$), and σ^2 denotes the noise level.

In this study, considering the priori information of reflectivity, an optimization problem with PD constraint can be formulated as

$$\min_{\mathbf{m} \in \mathbb{R}^n} \|P(\mathbf{m}) - P(\mathbf{m}^0)\|_p^p, \text{ s.t. } \|\mathbf{d} - \mathbf{d}_{obs}\|_2^2 \leq \sigma^2, \quad (7)$$

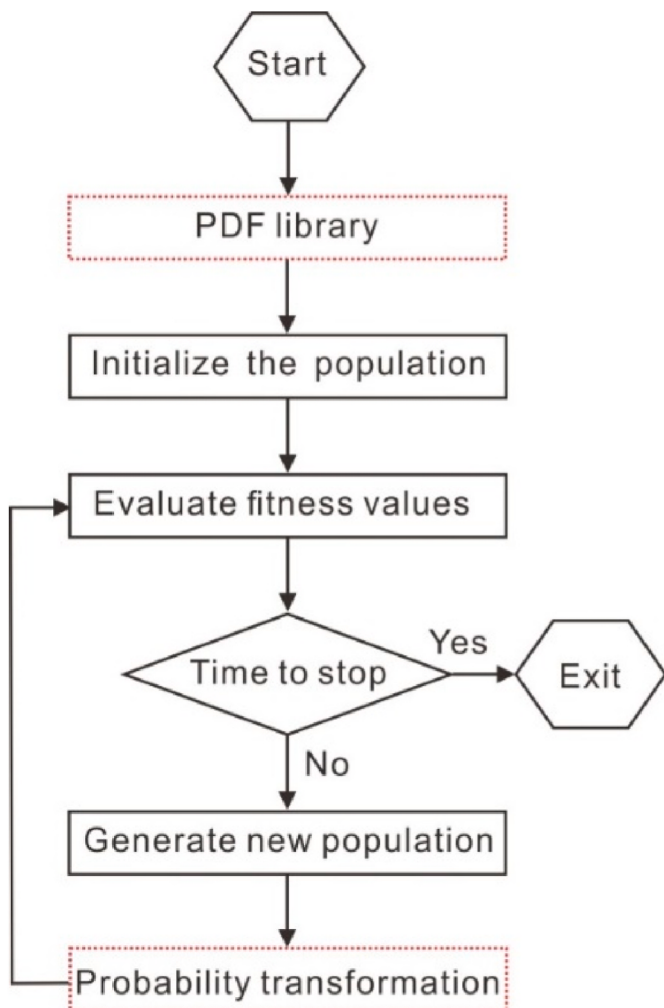


Fig. 1. Flowchart of SI algorithms. Two new operations are in the red dashed box.

where \mathbf{m}^0 is an a priori information of the reflectivity, and P denotes a probability density estimated from well logs. To maintain the same PD between \mathbf{m} and \mathbf{m}^0 , we proposed to apply a probability transformation in an updated global optimization approach. The implementation of the updated SI algorithms is presented in the next section.

2.2. SI algorithms with PD constraint

In general, standard SI algorithms should have three basic steps. In the first step, the initial population of agents is randomly generated from the solution representation. Each agent represents one solution. In the second step, each agent in the population is evaluated by the fitness value calculated by the misfit function. The fitness values of the population rank the agent within the population for selection. In the third step, a new population is updated by the perturbing of agents in the existing population.

In order to keep the same prior PDF of solutions in the optimization process, we proposed to improve the SI algorithms. As shown in Fig. 1, two extended operations (red dashed box), the PDF library and the probability transformation, are added. The updated SI algorithms with PD constraint usually have five basic steps.

The creating of the PDF library is the first step in the updated SI algorithms, as shown in Fig. 1. Before the original first step, we extract the PDF library of the parameter \mathbf{m}^{well} from the well logs. The PDF library is defined as

$$\Theta = \{m^{\text{well}} = [m_1, m_2, \dots, m_n]^T \mid m_i \in X, P(m_i = x_j) = p_j, i=1, 2, \dots, n; j=1, 2, \dots, k\} \quad (8)$$

where X and P denote a reflectivity sequence and its corresponding probability density. The form of X can be described as

$$X = \{x_1, x_2, \dots, x_k\}, \quad (9)$$

$$x_{j+1} = x_j + \Delta, \quad (10)$$

where Δ denotes a quantization parameter

$$\Delta = \frac{m_{\max} - m_{\min}}{k}, \quad (11)$$

where the m_{\min} and m_{\max} denote the minimum and the maximum of m^{well} , respectively. Then, the probability density P is written as

$$P = \{p_1, p_2, \dots, p_k\}, \quad (12)$$

$$p_j > 0, j = 1, 2, \dots, k, \quad (13)$$

$$\sum_{j=1}^k p_j = 1. \quad (14)$$

In the Equation (8), providing $n \gg k$, the parameter m^{well} has a sparse distribution.

The processing of the probability transformation is the fifth step in the updated SI algorithms, as shown in Fig. 1. After the original third step, in order to keep the PDF of the model parameter m and the PDF of the parameter m^{well} consistent, the probability transformation f can be defined as

$$m_{i,j}^k = f(m_{i,j,SI}^k), \quad (15)$$

where $m_{i,j,SI}^k$ denotes the model parameter calculated by the update of standard SI algorithms, and $m_{i,j}^k$ denotes the model parameter calculated by the probability transformation f . The probability transformation f is defined as

$$f = G^{-1}(P(m)), \quad (16)$$

where $P(m)$ is the PD of $m_{i,j,SI}^k$, and G is the probability distribution function of the reflectivity sequence. The form of the G can be defined as

$$G(x) = \int_{-\infty}^x p(\tau) d\tau. \quad (17)$$

In practice, we can calculate it using kernel method

$$G^{-1}(u) = \sum_{n=1}^k a_n \exp\left(-\frac{(u - u_n)^2}{2\sigma^2}\right), \quad (18)$$

$$u_n = G(x_n) = \frac{\text{number}(x \leq x_n)}{k} \quad (19)$$

$$a = (D + \sigma I)^{-1} x, \quad (20)$$

where D is the kernel matrix with the element $d_{ij} = \exp\left(-\frac{(u_i - u_j)^2}{2\sigma^2}\right)$, $x = [x_1, \dots, x_k]^T$, $\sigma > 0$ is a regularization parameter, I is the identity matrix. Mathematically, our proposed PD constraint is independent on a specific SI algorithm. In the other words, these two extended operations can be inserted into any standard SI algorithms. Considering the efficiency and popularity, the standard DE and PSO are chosen for updating in this study.

In the standard DE, the following are the main operators.

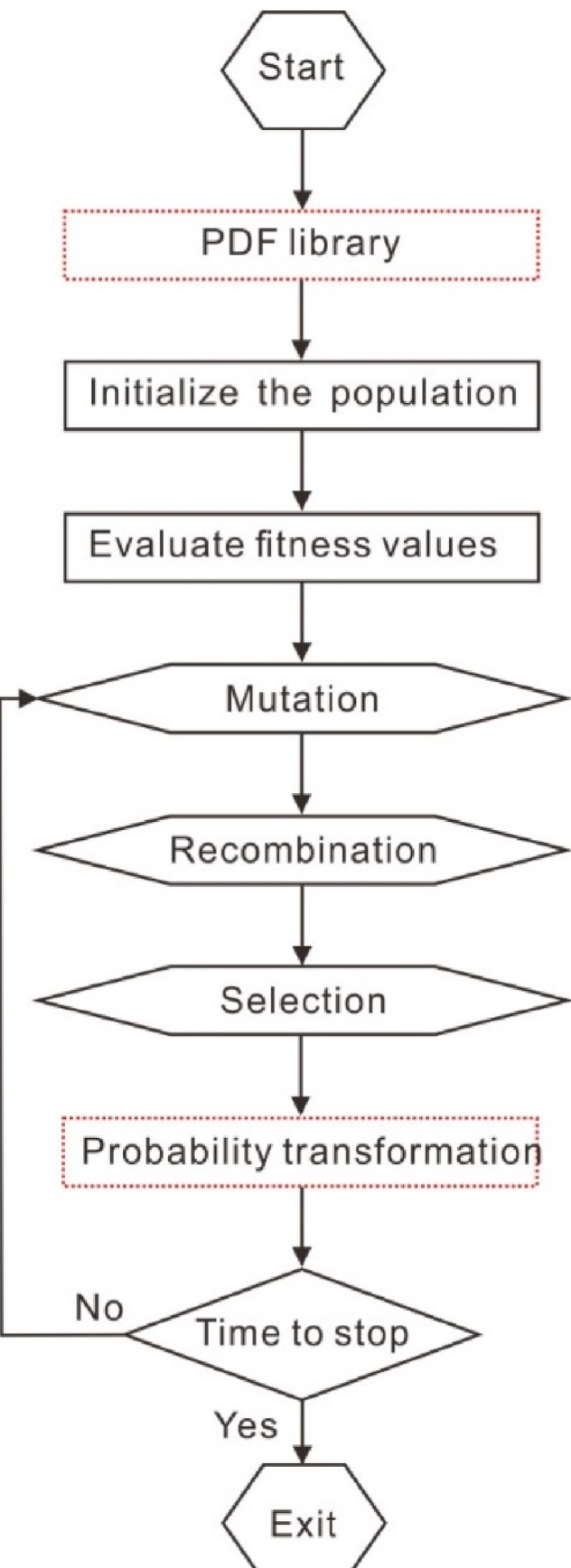


Fig. 2. Flowchart for DE. Two new operations are in the red dashed box.

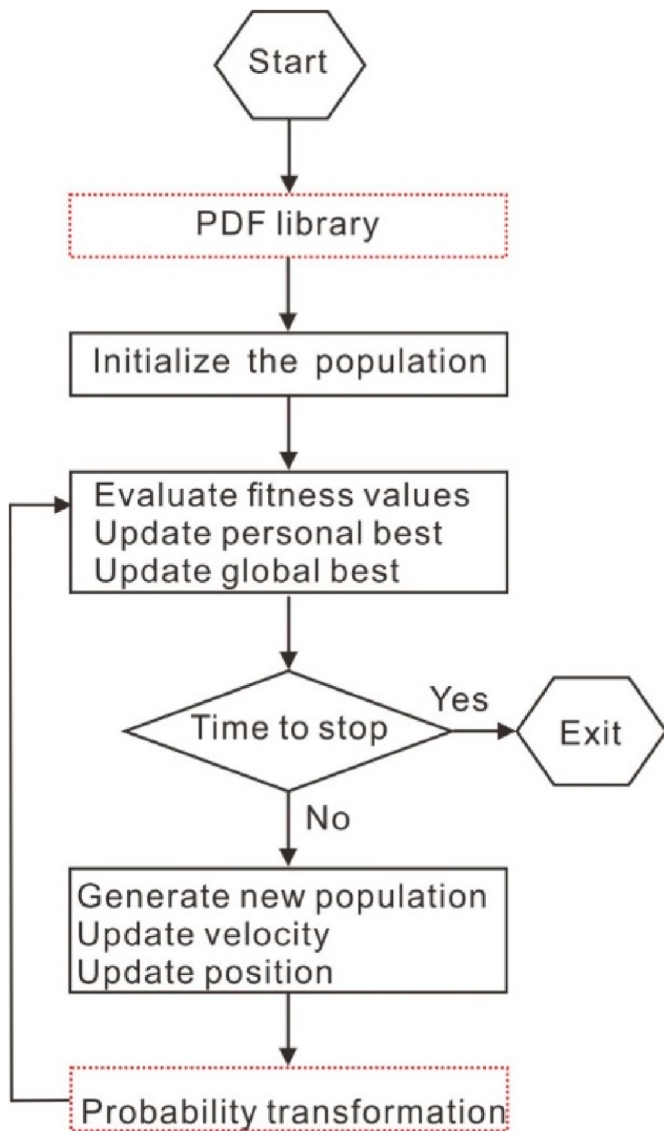


Fig. 3. Flowchart for PSO algorithms. Two new operations are in the red dashed box.

- 1) Mutation: For each vector X_i^k , select three vectors X_a^k , X_b^k and X_c^k randomly from the current population other than vector X_i^k . FM is mutation constant in $[0, 2]$. Generate a new population vector on the formula

$$X_i'^k = X_a^k + FM(X_b^k - X_c^k) \quad (21)$$

- 2) Crossover: Generate trial vectors applying the selected crossover scheme, i.e.

$$X_i'^k = \begin{cases} X_i'^k & \text{if } \text{rand} \leq C_R \\ X_i^k & \text{otherwise} \end{cases}, \quad (22)$$

where C_R is the crossover constant in $(0, 1)$.

- 3) Selection: Evaluate the trial vector and decide whether or not it will be part of the next generation by greedy strategy, i.e.

$$X_i^k = \begin{cases} X_i'^k & \text{if } \text{fitness}(X_i'^k) \geq \text{fitness}(X_i^k) \\ X_i^k & \text{otherwise} \end{cases}, \quad (23)$$

where $\text{fitness}()$ denotes the objective function.

In the standard PSO, the position and velocity of a particle, x_i and v_i , can be updated as follows:

$$v_i^{t+1} = v_i^t + \alpha \epsilon_1 [g^* - x_i^t] + \beta \epsilon_2 [x_i^* - x_i^t] \quad (24)$$

$$x_i^{t+1} = x_i^t + v_i^{t+1} \quad (25)$$

where ϵ_1 and ϵ_2 are two uniform random vectors within $[0, 1]$, α and β are acceleration constants, g^* denotes the current global best solution, and x_i^* denotes the individual best.

According to the scheme as shown in Fig. 1, the standard DE and PSO are easily improved to the DE-PD and PSO-PD. Figs. 2 and 3 show the updated workflows of DE-PD and PSO-PD, respectively. Note that the parameters of the original DE and PSO algorithms may be not be optimal in all numerical examples, because we prefer to show the advantages and disadvantages of the extended constraint of PD in the DE-PD and PSO-PD algorithms. Therefore, the parameters of four SI algorithms, such as the number of problem dimensions, the population, and the maximum iteration, should be set as the same for the next comparison in this study.

3. Numerical examples

3.1. 1-D model

We firstly use the case of a 1-D model numerical example to test the performance of four SI algorithms including the DE, the DE-PD, the PSO, and the PSO-PD. This model is a part of the Marmousi2 model (Martin et al., 2006) whose geological parameters are measured from the petroleum sedimentary basin.

Fig. 4(a) shows this 1-D velocity model with 700 m, which has been converted into the time domain by the travel time. For four SI algorithms, the number of problem dimension, the population, and the maximum iteration is 120, 40 and 200, respectively. The initial velocity model is random, which ranges from 1.0 km/s to 2.4 km/s. Using a 35-Hz Ricker wavelet, the results of the velocity inversion are shown in Fig. 4(a).

As shown in Fig. 4(a), the comparison of the velocity inversion by the DE (Yellow), the DE-PD (Red), the PSO (Cyan), and the PSO-PD (Magenta) with the true velocity, the mean errors are 0.5580, 0.3370, 1.0260 and 0.3876, respectively. In this model, we note that the PD of reflectivity is sparse (Fig. 4(b)). Due to the constraint of reflectivity PD, the convergence rates (fitness values) of the DE-PD and the PSO-PD are faster than the convergence rates of the DE and the PSO (Fig. 4(c)). Meanwhile, the fitness value of DE-PD is larger than that of PSO-PD in the first 30th iterations, and then the fitness value of DE-PD is smaller than that of PSO-PD in the next 170 iterations. Thus, the estimated velocity of DE-PD is better than the result of PSO-PD, while the runtime of DE-PD is longer than the runtime of PSO-PD.

As shown in Fig. 4(a), the interesting targets include a thick gas reservoir near 0.15 - 0.21 s and a thin oil reservoir near 0.92 - 0.93 s. The velocity reduces quickly at these gas and oil layers, where it is difficult to estimate the subsurface parameters accurately, seeing the results of the DE and the PSO. However, the results of DE-PD and PSO-PD can capture the lowest velocity in the thick gas layer. Especially, the DE-PD works well in the thin oil layer. Overall, the DE-PD performs best in the accuracy of estimation and convergence in this numerical case.

In addition, we add white Gaussian noise to the 1-D noise free inversion (synthetic seismic signal) to compare the robustness between the DE, the DE-PD, the PSO, and the PSO-PD. In this study, more than 100 independent trials are processed where the signal to noise-to-noise

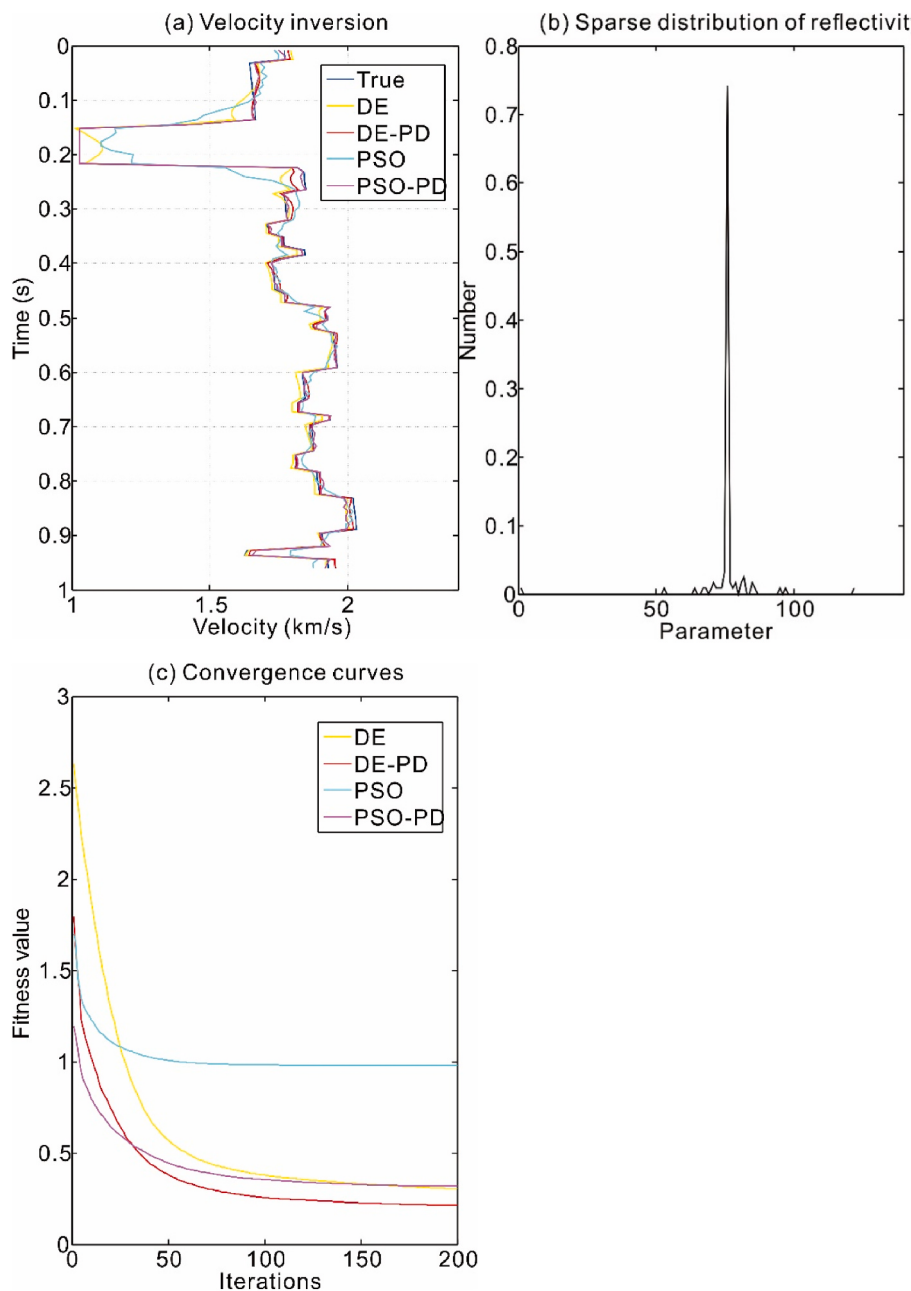


Fig. 4. A 1-D model numerical example. (a) Comparison of the estimated velocity by DE (Yellow), DE-PD (Red), PSO (Cyan), and PSO-PD (Magenta) with the true velocity, the mean errors are 0.5580, 0.3370, 1.0260 and 0.3876, respectively. (b) The PDF of 1-D reflectivity model is a sparse distribution. (c) Convergence curves of DE (Yellow), DE-PD (Red), PSO (Cyan), and PSO-PD (Magenta).

Table 1
Performance comparison of DE, DE-PD, PSO, and PSO-PD. The results are averaged over 100 independent trials.

	DE	DE-PD	PSO	PSO-PD
Runtime (s)	19.77	102.68	6.68	85.81
Fitness value	0.5322	0.3250	1.0013	0.4046
Mean error	0.3316	0.1555	0.7892	0.1834

ratio (SNR) level is a random value between 10 dB and 20 dB. The parameters of four SI algorithms are the same as those of noise free inversion.

The results of more than 100 independent experiments are shown in Table 1. The results of runtime, fitness and error are the average of several independent trials. In order to reduce the time cost in the more

than 100 independent trials, we adopted the parallel computation of multi-core processor.

As shown in Table 1, the runtime of DE-PD (102.68 s) is five times as large as that of DE (19.77 s), the fitness value of DE-PD (0.3250) is approximately two less than that of DE (0.5322), and the mean error of DE-PD (0.1555) is two times less than that of DE (0.3316). Similarly, the runtime of PSO-PD (85.81 s) is almost 13 times as large as that of PSO (6.68 s), the fitness value of PSO-PD (0.4046) is two less than that of PSO (1.0013), and the mean error of PSO-PD (0.1834) is four times less than that of PSO (0.7892). Totally, the DE-PD performs best in the accuracy of estimation and convergence, but its runtime is the largest. Thus, the long runtime of SI algorithms with PD constraint is one of the drawbacks in this study.

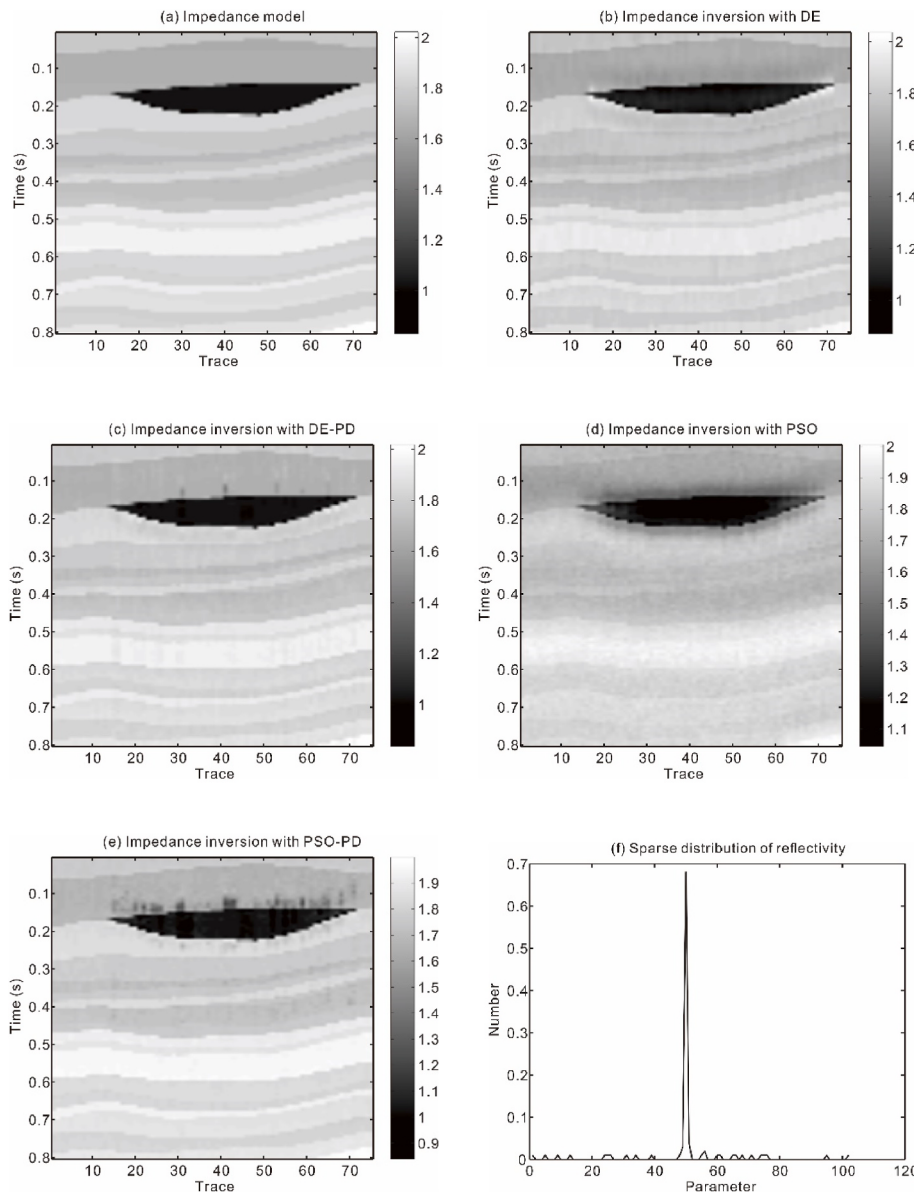


Fig. 5. Seismic impedances inversion of 2-D layer model. (a) 2-D impedance model is shown in time domain. Comparison of the 2-D impedance section estimated by (b) DE, (c) DE-PD, (d) PSO, and (e) PSO-PD with the true impedance model, the mean errors are 0.3582, 0.1986, 0.5115 and 0.3350, respectively. (f) The PDF of reflectivity is sparse. Interfaces of lens-shaped gas reservoir (black area) and multiple thin layers can be more clearly detected in the impedance estimated by the DE-PD.

3.2. 2-D layer model

We also estimate impedances of 2-D seismic section based on the part of the Marmousi2 model (Fig. 5(a)). In this 2-D layered model, the lowest impedance area (black lens) can be interpreted as a gas charged sand channel. As an example, this small-scale model has only 75 traces. The initial velocity model is random ranging from 1.0 km/s to 2.4 km/s. Due to multiple traces, we also adopted the parallel computing of multi-core processor to improve the computation speed of post-stacked seismic inversion with the known wavelet.

The compared results of four SI methods are shown in Fig. 5. The mean errors of them are 0.3582, 0.1986, 0.5115 and 0.3350, respectively. With the sparse distribution of the reflectivity model (Fig. 5(f)), the estimated seismic impedances of DE-PD and PSO-PD are better than the results of DE and PSO. Especially, the seismic impedance estimated by DE-PD shows the exact edges of the gas charged sand channel (black lens area) and several thin layers, as shown in Fig. 5(c).

Based on the comparison of the above numerical examples, we can mark three interesting points about our proposed method. (1) The DE-PD performs best in the accuracy of estimation and convergence among the four SI algorithms. (2) The early fitness value of DE-PD is

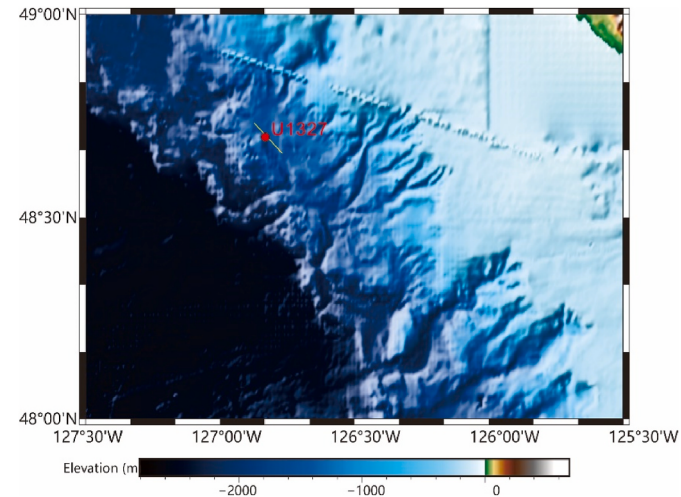


Fig. 6. Seismic experiment (yellow line) near IODP Site U1327 (red circle) on the Cascadia margin to study gas hydrates.

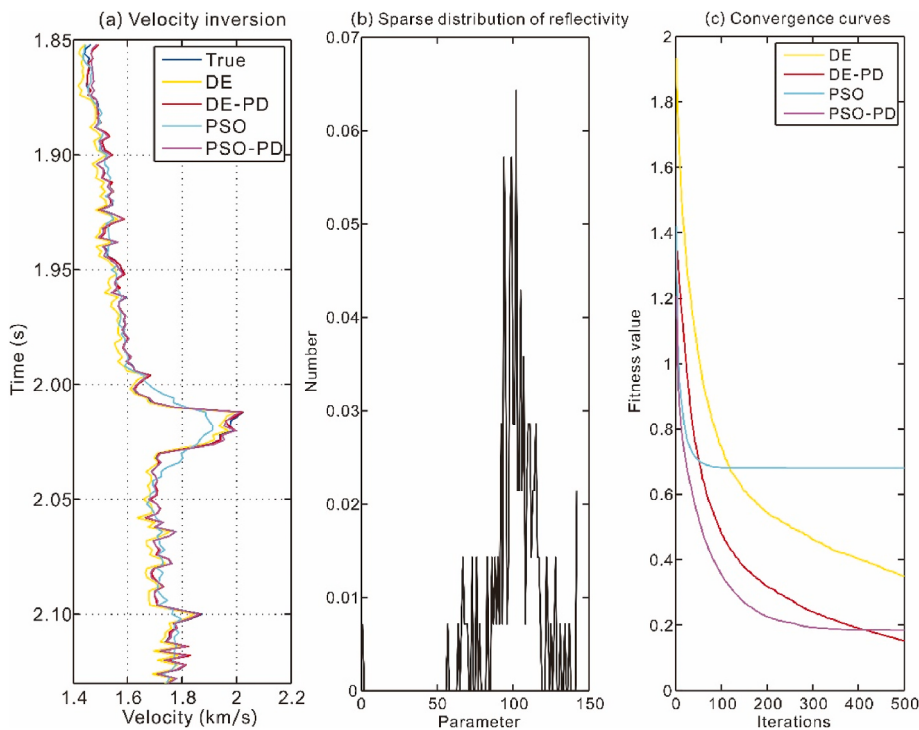


Fig. 7. A velocity inversion in the Site 1327 of IODP Expedition 311. (a) Comparison of the estimated velocity by DE (Yellow), DE-PD (Red), PSO (Cyan), and PSO-PD (Magenta) with the true velocity, the mean errors are 0.2801, 0.0699, 0.4225, and 0.0908 respectively. (b) The PDF of the reflectivity is sparse. (c) Convergence curves of DE (Yellow), DE-PD (Red), PSO (Cyan), and PSO-PD (Magenta).

larger than that of PSO-PD, and then the fitness value of DE-PD is smaller than that of PSO-PD in further iterations. (3) The runtime of DE-PD is the largest, and that of PSO-PD is the second.

3.3. Seismic inversion in Cascadia margin gas hydrates

Finally, we applied the SI algorithms to seismic inversion of seismic data acquired from a gas hydrates survey on the northern Cascadia margin offshore Vancouver Island, Canada. Detailed seismic reflection surveys have provided supporting data for gas hydrates on the northern Cascadia margin (Riedel et al., 2001). As shown in Fig. 6, seismic experiment and sites have been implemented by the IODP Expedition 311. It is significant to determine the origin of the bottom-simulating reflector (BSR) in the seismic reflection data (Yang et al., 2022). The BSR may indicate the base of the high velocity hydrate layer (Andreassen et al., 1997).

In this study, we focus on the IODP site U1327 (red circle) with a time interval from 1.85 s to 2.20 s. As shown in Fig. 7(a). Due to the high velocity, a typical BSR formation can be detected between 2.0 s and 2.05 s. For the gas hydrate sediments, the PDF of the reflectivity still is sparse (Fig. 7(b)).

For four SI algorithms, the number of problem dimension, the population, and the maximum iteration is 100, 40 and 300, respectively. The initial velocity model ranges from 1.4 km/s to 2.0 km/s. As shown in Fig. 7(a), comparing the estimated velocity by DE (Yellow), DE-PD (Red), PSO (Cyan), and PSO-PD (Magenta) with the true velocity, the mean errors are 0.2801, 0.0699, 0.4225, and 0.0908 respectively. Due to the constraint of sparse PD, accuracies of the DE-PD (Red) and the PSO-PD (Magenta) are higher than the original DE (Yellow) and PSO (Cyan) (Fig. 7(a)), while the convergence rates of the DE-PD and the PSO-PD are faster than convergence rates of the DE and the PSO (Fig. 7(c)). Compared with other methods, the DE-PD performs best both in the accuracy of estimation and convergence, which shows that the DE-PD is available to solve the seismic inversion for gas hydrate detection.

4. Conclusion

To keep the priori sparse distribution of reflectivity, we proposed the constrained scheme of seismic swarm intelligence inversion, especially two targeted DE-PD and PSO-PD algorithms. In this constrained scheme, due to the spatial stationarity of the sparse distribution of the reflectivity, a probability transformation is constructed, which can keep the distribution of model parameters as the same as the PDF library extracted from well logs. Under the same parameters, four SI algorithms, including DE, the DE-PD, the PSO, and the PSO-PD, are applied in marmousi2 and gas hydrates data. The results of velocity and impedance inversion show that the DE-PD and PSO-PD estimate better solutions than the conventional DE and PSO. In particular, the DE-PD performs best in terms of the accuracy of estimation and speed of convergence among the four SI algorithms. However, the main disadvantage of the DE-PD is the largest computation time. In the next, the proposed DE-PD will be accelerated by parallel computing with GPUs.

Funding

This work was supported by the National Natural Science Foundation of China (41974137).

Declaration of competing interest

The authors declare that they have no known competing financial interests or personal relationships that could have appeared to influence the work reported in this paper.

References

- Andreassen, K., Hart, P.E., MacKay, M., 1997. Amplitude versus offset modeling of the bottom simulating reflection associated with submarine gas hydrates. Mar. Geol. 137 (1–2), 25–40.
- Blum, C., Merkle, D. (Eds.), 2008. Swarm Intelligence. Springer Verlag, Berlin.

- Gao, Z.Q., Pan, Z.B., Gao, J.H., 2014. A new highly efficient differential evolution scheme and its application to waveform inversion. *IEEE Geosci. Rem. Sens. Lett.* 11 (10), 1702–1706.
- Gao, Z.Q., Pan, Z.B., Gao, J.H., 2016. Multimutation differential evolution algorithm and its application to seismic inversion. *IEEE Trans. Geosci. Rem. Sens.* 54 (6), 3626–3636.
- Gholami, A., Sacchi, M.D., 2015. A fast and automatic sparse deconvolution in the presence of outliers. *IEEE Trans. Geosci. Rem. Sens.* 50 (10), 4105–4116.
- Kazemi, N., Bongajum, E., Sacchi, M.D., 2016. Surface-consistent sparse multichannel blind deconvolution of seismic signals. *IEEE Trans. Geosci. Rem. Sens.* 54 (6), 3200–3207.
- Kennedy, J., Eberhart, R.C., 1995. Particle swarm optimization. *Proc. IEEE Int. Conf. Neural Networks* 4, 1942–1948.
- Ma, X., 2002. Simultaneous inversion of prestack seismic data for rock properties using simulated annealing. *Geophysics* 67 (6), 1877–1885.
- Martin, G.S., Wiley, R., Marfurt, K.J., 2006. Marmousi2: an elastic upgrade for Marmousi. *Lead. Edge* 25 (2), 156–166.
- Pan, S., Yan, K., Lan, H., Badal, J., Qin, Z., 2020. Adaptive step-size fast iterative shrinkage-thresholding algorithm and sparse-spike deconvolution. *Comput. Geosci.* 134, 04343.
- Riedel, M., Spence, G.D., Chapman, N.R., Hyndman, R.D., 2001. Deep-sea gas hydrates on the northern Cascadia margin. *Lead. Edge* 20 (1), 87–109.
- Semnani, A., Kamyab, M., Rekanos, I.T., 2009. Reconstruction of one-dimensional dielectric scatterers using differential evolution and particle swarm optimization. *IEEE Geosci. Rem. Sens. Lett.* 6 (4), 671–675.
- Sen, M.K., Stoffa, P.L., 2013. *Global Optimization Methods in Geophysical Inversion*. Cambridge University Press, Cambridge, UK.
- Storn, R., Price, K., 1997. Differential evolution-A simple and efficient heuristic for global optimization over continuous spaces. *J. Global Optim.* 11, 341–359.
- Wang, C., Gao, J.H., 2012. High-dimensional waveform inversion with cooperative coevolutionary differential evolution algorithm. *IEEE Geosci. Rem. Sens. Lett.* 9 (2), 297–301.
- Wang, Y.F., 2011. Seismic impedance inversion using l1-norm regularization and gradient descent methods. *J. Inverse Ill-Posed Probl.* 18 (7), 823–838.
- Wang, Z., Zhang, B., Gao, J., Huo Liu, Q., 2018. A frequency-domain seismic blind deconvolution based on Gini correlations. *J. Geophys. Eng.* 15 (1), 286–294.
- Wardhana, S.G., Pranowo, W., 2022. Rock-physics modeling by using particle swarm optimization algorithm. *J. Appl. Geophys.* 202, 104683.
- Yang, Y., Gao, J., Wang, Z., Liu, N., 2022. Data-driven time-frequency method and its application in detection of free gas beneath a gas hydrate deposit. *IEEE Trans. Geosci. Rem. Sens.* 60, 5909713.
- Zhou, Q.B., Gao, J.H., Wang, Z.G., 2015. Sparse spike deconvolution of seismic data using trust-region based SQP algorithm. *J. Comput. Acoust.* 23 (4), 1540002.